THE JOURNAL OF PHYSICAL CHEMISTRY A
A JOURNAL OF THE AMERICAN CHEMICAL SOCIETY

pubs.acs.org/JPCA Article

New Photoelectron–Valence Electron Interactions Evident in the Photoelectron Spectrum of Gd_2O^-

Published as part of The Journal of Physical Chemistry virtual special issue "Daniel Neumark Festschrift".

Jarrett L. Mason, Hassan Harb, Ali Abou Taka, Caleb D. Huizenga, Hector H. Corzo, Hrant P. Hratchian,* and Caroline Chick Jarrold*

Cite This: *J. Phys. Chem. A* 2021, 125, 9892–9903 Read Online

ABSTRACT: Evidence of strong photoelectron–valence electron (PEVE) interactions has been observed in the anion photoelectron (PE) spectra of several lanthanide suboxide clusters, which are exceptionally complex from an electronic structure standpoint and are strongly correlated systems. The PE spectrum of Gd_2O^-, which should have relatively simple electronic structure because of its half-filled 4f subshell, exhibits numerous electronic transitions. The electron affinity determined from the spectrum is 0.26 eV. The intensities of transitions to excited states increase relative to the lower-energy states with lower photon energy, which is consistent with shakeup transitions driven by time-dependent electron–neutral interactions. A group of intense spectral features that lie between electron binding energies of 0.7 and 2.3 eV are assigned to transitions involving detachment of an electron from outer-valence σ_u and σ_g orbitals that have large Gd 6s contributions. The spectra show parallel transition manifolds in general, which is consistent with detachment from these orbitals. However, several distinct perpendicular transitions are observed adjacent to several of the vertical transitions. A possible explanation invoking interaction between the ejected electron and the high-spin neutral is proposed. Specifically, the angular momentum of electrons ejected from σ_u or σ_g orbitals, which is $l = 1$, can switch to $l = 0, 2$ with an associated change in the M_s of the remnant neutral, which is spin–orbit coupling between a free electron and the spin of a neutral.

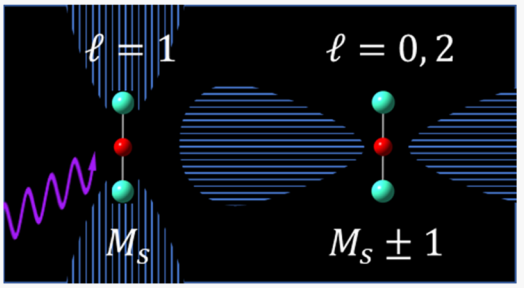

INTRODUCTION

With the ever-increasing need for faster, more efficient computational analysis and data storage, the development of practical quantum computing materials has been a central focus of a number of fields in the scientific community.[1−4] Of particular interest is the design of bi- or multi-stable magnetic species; these magnetic states, ideally, can be controlled by some external perturbation, like an electric field.[5,6] To this end, the lanthanides have proven to be enticing candidates because of their intrinsic large magnetic anisotropy and fascinating magnetic properties arising from the partially filled core-like 4f orbitals.[7,8] Fundamentally, the lanthanides (Ln) exhibit a rich manifold of nearly identical electronic states in a narrow energy window afforded by the partially occupied 4f orbitals and additional close-lying 6s and 5d orbitals. As an example, CeO ($4f^1\ \sigma_{6s}$) has 16 states within a 0.5 eV window of energy.[9−11]

We recently reported the effects of strong electron–neutral interactions in the photoelectron spectra of Sm_2O^- and $Gd_2O_2^-$.[12,13] Specifically, the probability of populating excited neutral states *via* anion detachment increased relative to the ground-state neutral with decreasing photon energy and, therefore, decreasing photoelectron kinetic energy (e^-KE); this observation is opposite of what would be expected to arise from threshold effects.[14] Pronounced effects were observed in a number of Sm-rich suboxide clusters,[15,16] but it was not observed in homometallic Ce-homologues, which implicated the greater density of electronic states from Sm's $4f^5$ or $4f^6$ subshell occupancy, compared to Ce's lone 4f electron. The effects were attributed to shakeup transitions or inelastic scattering resulting from strong photoelectron–valence electron (PEVE) interactions. An enhancement of the effects with decreasing photon energy is explained by the corresponding increase in PEVE interaction time associated with a decrease in the photoelectron velocity.[12]

The exceptionally high density of electronic states in $Sm_xO_y^-$ anion and neutral suboxide clusters render them difficult to interrogate experimentally and computationally,[15−17] and the exact nature of the excited states of Sm_2O being populated because of PEVE interactions could not

Received: September 3, 2021
Revised: October 25, 2021
Published: November 3, 2021

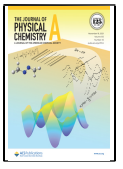

https://doi.org/10.1021/acs.jpca.1c07818
J. Phys. Chem. A 2021, 125, 9892–9903

readily be determined from the broad manifold of unresolved transitions observed in its anion PE spectrum.[12] In order to probe the nuances of the PEVE interactions in more detail, the photoelectron spectra of $Gd_2O_2^-$ were similarly examined over a range of photon energies.[13]

Relative to Sm_2O^-, $Gd_2O_2^-$ has a simpler electronic structure because the Gd-centers have half-filled $4f^7$ subshells and therefore zero orbital angular momentum (strictly speaking, they are not spherically symmetric),[18] and the incremental difference in oxidation state results in two fewer electrons in metal-local orbitals. $Gd_2O_2^-$, therefore, provided a canvas for exploring the fundamental physics of this effect. Our studies suggested the impact of two distinct PEVE interactions in which the electric field of the departing photoelectron (i) resulted in a time-dependent outer-valence orbital mixing which, in turn, provides an accessible route to increased population of excited neutral states as well as two-electron transitions observed in the spectra and (ii) affected the ordering of ferromagnetic (FM) and antiferromagnetic (AFM) states of the remnant neutral core. These effects have been observed in comparable physical systems described in the literature.[19−23]

Features in the PE spectra of $Gd_2O_2^-$ suggested a large axial zero-field splitting parameter (ca. −15 cm^{-1}) compared to typical sub-cm^{-1} coupling between Gd^{3+} centers in gadolinium complexes.[24] The higher coupling in the cluster anion may have a solution-phase analogue in Gd_2 complexes in which the Gd centers are coupled by radical anion bridging ligands.[25,26]

Herein, we report another example of PEVE interactions which give rise to inverse-threshold law behavior observed in our previous experiments but which also exhibit photoelectron angular distribution anomalies that point to additional PEVE-driven phenomena.

To lay the groundwork for understanding the electronic structure of Gd_2O/Gd_2O^-, DFT calculations on Gd_2O^- (*vide infra*) predict isoenergetic bent and linear Gd−O−Gd structures as the lowest-energy structures. As depicted in Figure 1, which shows the linear structure, the general electronic structure can be described as two Gd centers with $4f^76s^2$ electronic configurations, with the excess electron in a δ_g molecular orbital (MO) arising from the combination of the $5d_\delta$ orbitals. The occupancy of the δ_g orbital introduces nonzero overall orbital angular momentum, and spin−orbit splitting in the anion would favor the linear structure by ca. 1000 cm^{-1} relative to the bent structure.

A $^{16}\Delta_\Omega$ electronic term would result from FM coupled $4f^7$ centers; a $^2\Delta_\Omega$ term would arise from AFM coupled centers. Because the "outer-valence" $\delta_{g,5d}$ and $\sigma_{u,6s}/\sigma_{g,6s}$ orbitals are close in energy, numerous close-lying photodetachment transitions are anticipated and are observed, as will be described below. However, a new and exciting finding in the present study is the alternating opposite photoelectron angular distributions observed among the plethora of transitions. We propose that this may be another effect due to strong PEVE-driven transitions involving changes in the spin projection quantum number.

METHODS

Experimental Section. Gd_2O^- was generated and spectroscopically probed in an apparatus previously described in detail.[27−29] Briefly, a pressed Gd powder (Aesar, 99.9%) target was ablated with 7−9 mJ/pulse of the second harmonic output of an Nd:YAG laser (532 nm; 2.330 eV) operating at

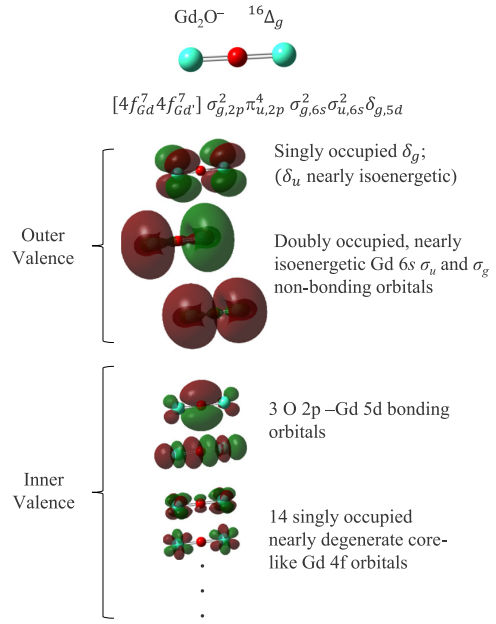

Figure 1. Molecular and electronic structure of Gd_2O^- calculated using DFT with a B3LYP hybrid density functional. The energy separation between the inner valence and outer valence orbitals is calculated to be 3.9 eV; detachment transitions observed in this study therefore involve only the outer valence electrons. Additional states found computationally are included in Table 2 and the Supporting Information.

30 Hz. The resulting plasma was swept by a pulse of He carrier gas into a 25 mm long, 3 mm diameter clustering channel, which allows clusters to form and cool to approximately room temperature. The clusters expanded into vacuum and were skimmed, and the anions were accelerated to 1 keV into a 1.2 m Bakker-style[30] time-of-flight mass spectrometer at the end of which is a dual microchannel plate (MCP) detector.

Gd_2O^- anions were photodetached before colliding with the ion detector using the second (532 nm; 2.330 eV) or third (355 nm; 3.495 eV) harmonic output of a second Nd:YAG laser. A small fraction (10^{-4}) of the photoelectrons traveled the length of an orthogonal 1 m field-free drift tube and were detected with a second dual MCP assembly. Electron drift times were recorded with a digitizing oscilloscope triggered by the detachment laser pulse and converted to electron kinetic energy (e^-KE), calibrated against other well-known PE spectra. The line width of transitions measured with this apparatus determined from atomic spectra[29] is e^-KE-dependent and given by

$$\Delta E = 0.004\ \text{eV} + 0.0078\ \text{eV}\cdot\left(\frac{e^-\text{KE}}{\text{eV}}\right)^{3/2} \quad (1)$$

The e^-KE associated with any given detachment transition is photon energy-dependent. To allow greater ease in comparison between spectra obtained with different photon energies, the spectra presented below are plotted in terms of the electron binding energy (e^-BE), which is the photon energy-independent relative energy between the initial anion and final neutral state:

$$e^-\text{BE} = h\nu - e^-\text{KE} = \text{EA} + E_{\text{int}}^{\text{neutral}} - E_{\text{int}}^{\text{anion}} \quad (2)$$

EA is the electron affinity of the neutral; $E_{\text{int}}^{\text{neutral}}$ is the internal energy of the neutral (electronic, vibrational, and rotational

https://doi.org/10.1021/acs.jpca.1c07818
J. Phys. Chem. A 2021, 125, 9892−9903

energy), and E_{int}^{anion} is similarly the internal energy of the anion. If the internal energy of the ion is low, only the lowest-energy vibronic levels of the anion will be populated, and the spectrum will primarily reflect energy levels of the neutral relative to the initial state (or energetically close-lying states) of the anion.

Spectra were accumulated for 6.24 million (2.330 eV spectrum) and 6.84 million (3.495 eV spectrum) laser shots at both vertical ($\theta = 0° \pm 10°$) and horizontal ($\theta = 90° \pm 10°$) detachment laser polarizations. Comparing the intensities of features between the two polarizations allows us to approximate the anisotropy parameter, β, according to the following equation:

$$\beta = \frac{(I_0 - I_{90})}{(0.5I_0 + I_{90})} \quad (3)$$

where I_0 and I_{90} are the intensities of electron yield for transitions in spectra obtained over the same number of laser shots (alternatingly over smaller collection times to minimize the effect of any drift in source conditions). As described cogently by Sanov,[31] in molecular systems, this parameter can give insight into the nature of the molecular orbitals from which the electrons are being detached. Typically, $\beta = 2$ is associated with detachment from predominately s-type molecular orbitals, and $\beta < 0$ indicates significant p-type orbital character. Purely isotropic photoelectron angular distributions (PADs) can also be attributed to electron ejection *via* an indirect process, such as thermionic emission.

Computational Methods. Calculations were carried out using the Gaussian suite of electronic structure programs[32] and employed the B3LYP/ANO-ECPplusPVTZ model chemistry. The ANO-ECPplusPVTZ incorporates the Stuttgart relativistic small-core atomic natural orbital basis set and effective core potential and corresponding valence basis set for Gd,[33] which implicitly incorporates some degree of spin−orbit effects in the scalar-relativistic pseudopotentials, and a Dunning-style correlation consistent basis set for O.[34] All converged Kohn−Sham determinants were characterized using stability calculations. Geometry optimizations were carried out using standard techniques, and potential energy surface stationary points were characterized using analytic second-derivative calculations.[35,36] Reported energies include zero-point energy corrections.

In order to facilitate convergence for challenging electronically excited states, the projected initial maximum overlap method (PIMOM) was used. PIMOM is a variation of the initial maximum overlap method (IMOM) developed by Gill et al.[37,38] and has been implemented in a local development version of Gaussian.[39] More specifically, this method drives self-consistent field convergence toward challenging electronic structures using an initial guess from the ground-state molecular orbitals and a projected overlap metric.

For molecules exhibiting complex electronic structure, specifically when energy gaps between electronic states are quite small, multideterminantal wave functions might be a better representation of the true electronic structure than using Kohn−Sham (KS) DFT. With this in mind, KS DFT results must be used with care. This has been achieved through evaluation of KS determinant stability and spin-squared expectation values. Indeed, evaluating anion−neutral energy gaps and Franck−Condon simulations using such DFT methods yielded results that are in very good agreement with experimental spectra, which in turn facilitated the assignment of spectral peaks and the determination of the molecular and electronic states that are present in the experimental photoelectron spectra.

The simplest points of comparison between the computational and experimental results are the adiabatic EA (EA_a), adiabatic detachment energies (ADE), and the vertical detachment energies (VDE). The calculated EA_a is the energy difference between the zero-point levels of the neutral and anion ground states. The ADE is the same applied to any electronic transition and correlates with the origin of the transition. The VDE is the energy at which the transition reaches maximum intensity (i.e., Franck−Condon overlap) and is the difference in energy between the anion and the neutral confined to the geometry of the anion.

A more detailed comparison between the computational and experimental results involves a simulation of the vibrational structure of a transition, based on the structures, vibrational frequencies, and normal coordinates of the anion and neutral. A more detailed description of the home-written simulation code was provided previously.[40]

RESULTS AND DISCUSSION

Along the lanthanide series, the properties of adjacent elements are very similar. The incremental increase in 4f subshell occupancy, which increases nuclear shielding, results in similar effective nuclear charges for neighboring elements, leaving the outer-valence electrons to govern very similar chemical and physical properties.[41] However, as will be shown, there are distinct differences in the electronic structures in several Ln_2O anion and neutral molecules that can be attributed to differences in the spin−orbit coupling associated with different 4f subshell occupancies.

Anion PE Spectrum of Gd_2O^- and Comparison to Ce_2O^- and Sm_2O^-. Figure 2 shows the PE spectra of (a) Ce_2O^-, (b) Sm_2O^-, and (c) Gd_2O^-, collected using 3.495 eV (blue) and 2.330 (green) photon energies, with the electric field polarization parallel (dark colors) and perpendicular (light colors) to the electron drift path. The Ce_2O^- and Sm_2O^- spectra were published previously[12,15,42] and are included here for direct comparison. The lowest-energy transitions in the Ce_2O^- and Sm_2O^- spectra, labeled **X**, are intense and have parallel PADs typical of detachment from 6s-based molecular orbitals.[42−44] The spectra are qualitatively similar in appearance. Bands **X**, **A**, and **B** in the Sm_2O^- spectrum are not three individual electronic transitions. Rather, they are manifolds of close-lying transitions associated with a common detachment process (e.g., detachment of an electron from the HOMO) but differing in terms coupling between the $4f^6$ (^7F) centers on the two Sm atoms. Note that the ratio of the integrated intensities of band **A** to band **X** is significantly higher in the spectrum obtained with 2.330 eV photon energy, an effect attributed to the strong PEVE interactions noted in the Introduction. Band **X** in the spectra of both Ce_2O^- and Sm_2O^- is assigned to states accessed by detaching electrons from the outer-valence MOs with 6s character.

The PE spectrum of Gd_2O^- is strikingly different from the Ce_2O^- and Sm_2O^- spectra. In both the spectra collected with 3.495 and 2.330 eV photon energies, numerous transitions lie between 0.7 and 2.3 eV, labeled **X**, **A**, **B**, **C**, and **D**. Peak positions are summarized in Table 1. As with the Sm_2O^- spectrum, these features appear to be manifolds of electronic transitions rather than five individual transitions, and features within each band are partially resolved. Bands **B**, **C**, and **D**

https://doi.org/10.1021/acs.jpca.1c07818
J. Phys. Chem. A 2021, 125, 9892−9903

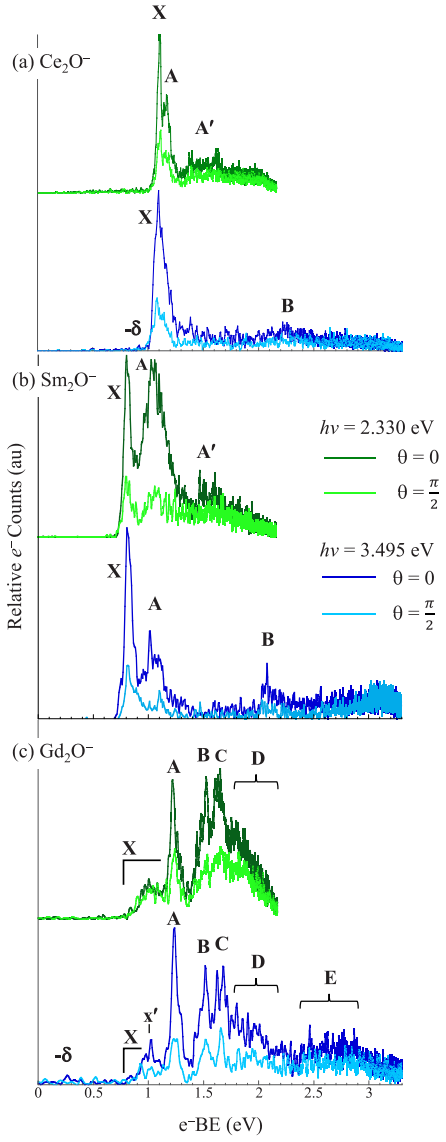

Figure 2. Anion PE spectra of (a) Ce_2O^-, (b) Sm_2O^-, and (c) Gd_2O^- measured using 2.330 eV (green traces) and 3.495 eV (blue traces) photon energies. Darker colors are spectra measured with the laser polarization parallel to the electron drift path; lighter traces represent perpendicular polarization. Part a is reprinted with permission from ref 42. Copyright 2016 AIP Publishing. Part b is reprinted with permission from ref 15. Copyright 2017 AIP Publishing.

increase in relative intensity in comparison to bands **X** and **A** in the spectrum collected with 2.330 eV photon energy, which points to PEVE interactions.

Band **X** in the PE spectrum of Gd_2O^- is relatively low-intensity and broadened, while the more intense, parallel feature (**A**) is comparable to band **X** in the Ce_2O^- and Sm_2O^- spectra. Irregular peak spacings within band **A** are discerned in the spectrum obtained with 2.330 eV, and their positions are summarized in Table 1. At higher e⁻BE, the congested features grouped into portions labeled **B**, **C**, **D**, and **E**, in addition to a considerable continuum signal, do not readily correlate with features in the two other Ln_2O^- spectra shown. The fact that the spectrum of Gd_2O^- is more congested with electronic transitions is unexpected. As noted in the Introduction, the $4f^7$ (^8S) centers on the two Gd centers in Gd_2O^-, in contrast to

Table 1. Positions of Bands, or Any Partially Resolved Peaks within Those Bands, along with the Angle Relative to the Laser Polarization at Which the Signal Is More Intense, Observed in the PE Spectra of Gd_2O^-[a]

band	e⁻BE (eV)		tentative assignment
−δ[b]	0.26 ± 0.02(∥)	signal at this energy in 2.330 eV spectrum indistinguishable from noise	$^{15}\Sigma_g-^{16}\Delta_g$
X[c]	0.84 ± 0.02(∥)		$^{17}B_2-^{16}\Delta_g$
	0.90 ± 0.02(⊥)		
	0.94 ± 0.02(∥)		
	0.97 ± 0.02(∥)		
	1.00 ± 0.01(∥)[b]		
	1.08 ± 0.03 (isotropic)		
A[c]	1.16 ± 0.02(⊥)		$^{17}\Delta_u-^{16}\Delta_g$
	1.22 ± 0.02(∥)		
	1.24 ± 0.02(⊥)		
	1.26 ± 0.02(∥)		
	1.29 ± 0.02(∥)		
	1.31 ± 0.02(∥)		
B[c]	1.43 ± 0.04 (⊥)		($^{15}B_2-^{16}\Delta_g$ contributes to continuum signal)
	1.44 ± 0.02(∥)		
	1.48 ± 0.02(∥)		
	1.53 ± 0.02(∥)		$^{17}\Delta_g-^{16}\Delta_g$
C[b]	1.62 ± 0.03(∥)	features broadened and less resolved in the 2.330 eV spectrum	$^{15}\Delta_u-^{16}\Delta_g$
	1.66 ± 0.03(⊥)		
	1.68 ± 0.03(∥)		
D[c]	1.7−2.1 (∥)		$^{15}\Delta_g-^{16}\Delta_g$
E[b]	**2.42 ± 0.03**(∥)		
	2.5−3.0 (isotropic)		

[a]The most intense peak within each band is in **bold** font. Tentative assignments based on computational results are included. [b]Feature better resolved or only observed in the 3.495 eV PE spectrum; position is based on this spectrum. [c]Feature better resolved in the 2.330 eV PE spectrum; position is based on this spectrum.

the $4f^6$ (^7F) centers in Sm_2O^-, do not introduce numerous close-lying spin−orbit states present in Sm_2O/Sm_2O^-.

There are several subtle differences between the spectra of Gd_2O^- obtained with the two photon energies. Band **X** in the spectrum collected with 3.495 eV (blue trace) is punctuated by a narrow feature labeled **x′** at e⁻BE = 1.00 ± 0.01 eV, with parallel PAD. In the spectrum obtained with 2.330 eV, band **X** has *overall* more isotropic (*vide infra*) PAD. In addition, bands **C** and **D** observed in the spectrum collected with 2.330 eV should be better resolved than the same features in the spectrum collected with 3.495 eV per eq 1. Instead, these bands appear broadened in the 2.330 eV spectrum relative to the 3.495 eV spectrum.

A reproducible and unusual effect evident in the spectra obtained with the laser polarization parallel and perpendicular to the direction of electron collection is opposite PADs exhibited by adjacent, close-lying transitions. This effect is observed in spectra collected with both 2.330 and 3.495 eV photon energies, but it is more distinct in the former because the transitions are better resolved (again, eq 1). The 2.330 eV spectrum is shown on an expanded scale in Figure 3a with contrasting colors (green and red) used to illustrate the differences. Figure 3b shows a narrower e⁻BE range, with the spectrum collected with perpendicular polarization scaled by a factor of 2 to facilitate comparison. On the low e⁻BE edge of

https://doi.org/10.1021/acs.jpca.1c07818
J. Phys. Chem. A 2021, 125, 9892−9903

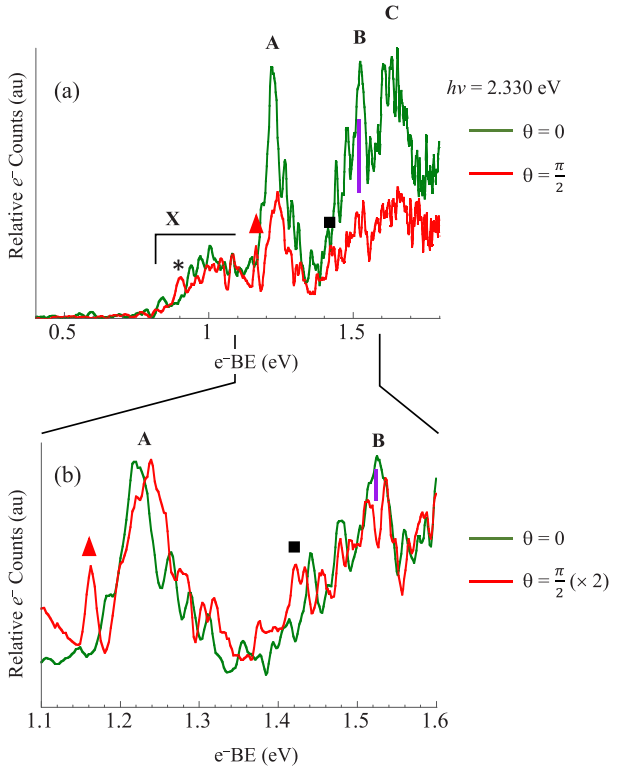

Figure 3. (a) Anion PE spectrum of Gd_2O^- measured using 2.330 eV photon energy shown on an expanded scale and with more contrasting colors to distinguish between the parallel (green) and perpendicular (red) polarizations. (b) Close-up of the 1.1−1.6 eV range, with the perpendicular spectrum scaled by a factor of 2, demonstrating distinct differences in spectral profiles between the spectra taken with different polarization.

bands **X**, **A**, and **B**, distinct peaks are observed in the perpendicular spectrum, labeled with symbols, that coincide with a local intensity minimum in the parallel spectrum. Band **C** in the spectrum obtained with 2.330 eV is more congested than the same band in the 3.495 eV spectrum, which shows a distinct maximum intensity in the spectrum measured with perpendicular polarization at a local minimum in the parallel analogue, as can be seen in Figure 2c.

This observation supports the assertion that these bands are manifolds of close-lying, but distinct, electronic transitions, but the striking difference in PAD across these manifolds suggests that transitions within them involve detachment from orbitals of different symmetry. Electronic structure calculations on Gd_2O^- and Gd_2O were therefore conducted to support interpretation of the anomalous PADs observed in the spectra.

Computed Electronic Structures of Gd_2O^- and Gd_2O and Spectral Assignments. Results of calculations on the Gd_2O anion and neutral suggest a high density of electronic states, a sampling of which are summarized in Table 2. A more comprehensive list of states is included in the Supporting Information. Neutral states that are accessible by one-electron detachment transitions from any of the anions bound with respect to the e^- + neutral continuum are separated from neutral states that are not (*i.e.*, orbital occupancies that differ by more than one electron from the bound anions). Several structural parameters and representative vibrational frequencies are included. We note that Gd−Gd−O structural arrangements were not energetically competitive with Gd−O−Gd bridge-bound structures, and calculations on the Gd−Gd−O initial structure tended to converge to the bridged structure. Linear and bent structures converged for the neutral. In general, the bend mode for all of the structures is low-frequency ($\lesssim$100 cm^{-1}). The Gd−O symmetric stretch is not expected to be active in any of the anion-to-neutral transitions; the difference between the anion and neutral Gd−O bond distances are at most approximately 0.03 Å. The symmetric stretch frequency in the linear structures is approximately 200 cm^{-1} in linear molecules, low because it involves motion of the heavy Gd centers, while it is higher-frequency in the bent structures (ca. 480 cm^{-1}), as it involves motion of the O-atom relative to the two Gd centers.

Ground States of the Anion and Neutral. As noted in the Introduction, bent and linear Gd−O−Gd structures of the anion were predicted to be isoenergetic (within <0.001 eV) with the B3LYP/ANO-ECPplusPVTZ method. Both can be described as having the same electronic structures illustrated in Figure 1, though the bent structure features some overlap between the two terminal 5d orbitals with a $^{16}A_1$ electronic term. When using Douglas−Kroll−Hess second-order relativistic integrals,[45] rather than an effective core potential, the bent structure is predicted to be slightly more stable by 0.03 eV. To examine if this small preference for the bent geometry is dependent on the use of the B3LYP functional, we also carried out the same computational experiment using the Douglas−Kroll−Hess second-order relativistic integrals with the B3PW91 functional.[46] In that case, the bent structure is still favored. Using B3PW91, the bent structure is more stable than the linear structure by 0.15 eV. Nevertheless, the combination of greater charge delocalization[12,15,42,43,47−50] and spin−orbit coupling in the linear structure suggests it is more stable. For a sense of scale, the spin−orbit components of the 6s 5d state of Gd^+ span approximately 0.23 eV.[51] While the analogous splitting in Gd_2O^- may be lower, this splitting exceeds the highest computed difference in bent to linear energy. However, because both the bent and linear structures are local minima, the bend potential could be rather complicated with strong vibronic coupling.

The EA of the neutral is calculated to be 0.28 eV, which is much lower in energy than most of the signal observed in the spectrum. The lowest-energy neutral state is a linear $^{15}\Sigma_g$ state, which is one-electron accessible from detachment of the single electron in the δ_g orbital of the $^{16}\Delta_g$ state. A low-intensity signal is observed in the Gd_2O^- spectrum measured using 3.495 eV photon energy at 0.26 eV, labeled "-δ," which we attribute to the $^{15}\Sigma_g \leftarrow {}^{16}\Delta_g$ transition based on this computational result, as indicated in Table 1. This transition is predicted to be at a much lower energy than the analogous transition in the Ce_2O^- spectrum (Figure 2a). In contrast to the calculated relative orbital energies shown in Figure 1, calculations on Ce_2O^- predicted the (singly occupied) 5d-based MOs to lie below the $b_{2,6s}$ orbital, which correlates to the σ_u orbital in Figure 1.[42] The differences in relative energies of analogous MOs is not unexpected, given the differences in orbital occupancies of the atomic systems. For example, the atomic Ce^- orbital occupancy is $4f\ 5d^2\ 6s^2$, while the Gd^- occupancy is $4f^7\ 5d\ 6s^2\ 6p$.[52]

As noted in earlier studies on lanthanides and lanthanide oxides, the cross section for detachment of electrons from MOs with 4f or 5d character is very small compared to the cross section for detachment from MOs with 6s character.[29,42,53] Therefore, the more intense features are associated with detaching electrons from either of the close-lying σ_g and

https://doi.org/10.1021/acs.jpca.1c07818
J. Phys. Chem. A 2021, 125, 9892−9903

Table 2. Summary of Several of the Electronic States Calculated for Gd_2O^- and Gd_2O[a]

	molecular term	electronic configuration (O 2p orbitals omitted)	relative energy (eV)	Gd−O (Å)	∠Gd−O−Gd	vibrational frequencies (cm^{-1}) ν_1, ν_2, ν_3†
Gd_2O $2e^-$ accessible from bound states of anion	$^{15}\Gamma_g$ (5d)	$4f_a^{7\alpha}4f_b^{7\alpha}...\sigma_g^{\beta}\sigma_u^{\alpha}\delta_g^2$	3.53			
	$^{17}\Sigma_u$ (5d)	$4f_a^{7\alpha}4f_b^{7\alpha}...\sigma_g^2\sigma_u^{\alpha}\sigma_{g,5d}^{\alpha}$	3.37			
	$^{15}\Pi_u$ (5d)	$4f_a^{7\alpha}4f_b^{7\alpha}...\sigma_g^{\beta}\sigma_u^2\pi_{u,5d}^{\alpha}$	3.19			
	$^{15}\Gamma_u$ (5d)	$4f_a^{7\alpha}4f_b^{7\alpha}...\sigma_g^{\beta}\sigma_u^{\beta}\delta_u^{\alpha}\delta_g^{\alpha}$	2.90			
	$^{17}\Phi_u$ (6p)	$4f_a^{7\alpha}4f_b^{7\alpha}...\sigma_g^2\delta_u^{\alpha}\pi_{u,6p}^{\alpha}$	2.80			
	$^{17}\Sigma_g$ (6p)	$4f_a^{7\alpha}4f_b^{7\alpha}...\sigma_g^{\alpha}\sigma_u^2\sigma_{g,6p}^{\alpha}$	2.55			
	$^{15}\Pi_u$ (6p)	$4f_a^{7\alpha}4f_b^{7\alpha}...\sigma_g^{\beta}\sigma_u^2\pi_{u,6p}^{\alpha}$	2.35			
	$^{17}\Pi_g$ (5d)	$4f_a^{7\alpha}4f_b^{7\alpha}...\sigma_g^2\sigma_u^{\alpha}\pi_{u,5d}^{\alpha}$	2.31			
	$^{17}\Gamma_u$ (5d)	$4f_a^{7\alpha}4f_b^{7\alpha}...\sigma_g^2\delta_u^{\alpha}\delta_g^{\alpha}$	2.22			
	$^{17}\Sigma_u$ (6p)	$4f_a^{7\alpha}4f_b^{7\alpha}...\sigma_g^2\sigma_u^{\alpha}\sigma_{g,6p}^{\alpha}$	2.12*			
	$^{17}\Pi_u$ (6p)	$4f_a^{7\alpha}4f_b^{7\alpha}...\sigma_g^{\alpha}\sigma_u^2\pi_{u,6p}^{\alpha}$	2.02			
	$^{15}\Pi_g$ (6p)	$4f_a^{7\alpha}4f_b^{7\alpha}...\sigma_g^2\sigma_u^{\beta}\pi_{u,6p}^{\alpha}$	1.98			
	$^{17}\Pi_g$ (6p)	$4f_a^{7\alpha}4f_b^{7\alpha}...\sigma_g^2\sigma_u^{\alpha}\pi_{u,6p}^{\alpha}$	1.58*			
Gd_2O $1e^-$ accessible from ***bound*** states of anion	$^{13}\Delta_g$	$4f_a^{7\alpha}4f_b^{7\alpha}...\sigma_g^{\beta}\sigma_u^2\delta_g^{\beta}$	2.53			
	$^{15}\Delta_g$	$4f_a^{7\alpha}4f_b^{7\alpha}...\sigma_g^{\alpha}\sigma_u^2\delta_g^{\beta}$	2.50			
	$^{15}\Delta_u$	$4f_a^{7\alpha}4f_b^{7\alpha}...\sigma_g^{\beta}\sigma_u^2\delta_u^{\alpha}$	2.20			
	$^{15}\Delta_g$	$4f_a^{7\alpha}4f_b^{7\alpha}...\sigma_g^{\beta}\sigma_u^2\delta_g^{\alpha}$	2.04			
	$^{17}\Delta_g$	$4f_a^{7\alpha}4f_b^{7\alpha}...\sigma_g^{\alpha}\sigma_u^2\delta_g^{\alpha}$	1.62		180	
	$^3\Delta_g$	**$4f_a^{7\alpha}4f_b^{7\beta}...\sigma_g^2\sigma_u^{\alpha}\delta_u^{\alpha}$**	**1.57**		**108**	
	$^{17}\Delta_g$	$4f_a^{7\alpha}4f_b^{7\alpha}...\sigma_g^2\sigma_u^{\alpha}\delta_u^{\alpha}$	1.38		180	
	$^{15}B_2$; $^{15}\Delta_u$	$4f_a^{7\alpha}4f_b^{7\alpha}...\sigma_g^2\sigma_u^{\beta}\delta_g^{\alpha}$	1.30; 1.66		105; 180	
	$^3\Delta$	**$4f_a^{7\alpha}4f_b^{7\beta}...\sigma_g^2\sigma_u^{\alpha}\delta_g^{\alpha}$**	**0.96**	2.054; 1.957	180	781, 192, 71†
	$^{17}B_2$; $^{17}\Delta_u$*	$4f_a^{7\alpha}4f_b^{7\alpha}...\sigma_g^2\sigma_u^{\alpha}\delta_g^{\alpha}$	0.95; 1.22*	2.011; 1.988	106; 180	511, 100, 482; 196, 677, 78*i*†
	$^1\Sigma_g$	**$4f_a^{7\alpha}4f_b^{7\beta}...\sigma_g^2\sigma_u^2$**	**0.28**	1.989	180	202, 798, 92†
	$^{15}\Sigma_g$	$4f_a^{7\alpha}4f_b^{7\alpha}...\sigma_g^2\sigma_u^2$	0.28	1.990	180	201, 797, 93†
Gd_2O^-	$^{14}\Delta_g$	$4f_a^{7\alpha}4f_b^{7\alpha}...\sigma_g^2\sigma_u^2\delta_g^{\beta}$	0.67* (not bound)		–	
	$^{16}\Pi_u$	$4f_a^{7\alpha}4f_b^{7\alpha}...\sigma_g^2\sigma_u^2\pi_u^{\alpha}(6p)$	0.35 (not bound)		180	
	$^{16}\Delta_u$	$4f_a^{7\alpha}4f_b^{7\alpha}...\sigma_g^2\sigma_u^2\delta_u^{\alpha}$	0.18*		–	
	$^2\Delta$	**$4f_a^{7\alpha}4f_b^{7\beta}...\sigma_g^2\sigma_u^2\delta_g^{\alpha}$**	**0.14**	2.140; 1.917	180	728, 167, 54†
	$^{16}A_1$;$^{16}\Delta_g$	$4f_a^{7\alpha}4f_b^{7\alpha}...\sigma_g^2\sigma_u^2\delta_g^{\alpha}$	0; 0	2.017; 2.008	123; 180	428, 55, 461
						190, 404, 33†

[a]A comprehensive list is provided in the Supporting Information. Shaded boxes indicate one-electron accessible states from the ground $^{16}\Delta_g$ state of the anion. Asterisks (*) indicate energies determined from single-point calculations when structure optimizations failed to converge. Daggers (†) indicate the degenerate π_u modes for the linear species. States shown in **bold** font are AFM-coupled states. The molecular terms for states that are accessible only *via* shake-up transitions include the AO-basis of the electron excitation accompanying detachment.

σ_u orbitals (Figure 1). Calculations predict these transitions to lie at e^-BE values between 0.95 and 2.04 eV, the energy interval in which numerous detachment transitions are observed experimentally. In a simple one-electron picture, there would be only four transitions originating from the $^{16}\Delta_g$ state in this energy range, as there are four electrons occupying the σ_g and σ_u orbitals. The spectrum, on the other hand, is congested with numerous partially resolved transitions.

Excited States of the Anion. Low-lying electronic states of the anion may contribute to the number of observed transitions. Excited anionic states, calculated using PIMOM, were found by promoting an electron from the δ_g to the δ_u orbital ($^{16}\Delta_u$; T_0 = 0.18 eV) or flipping the spin of the δ_g electron relative to the high-spin 4f cores ($^{14}\Delta_g$; T_0 = 0.67 eV, not bound with the calculated detachment continuum). The low excitation energy of the $^{16}\Delta_u$ state reflects the weak coupling between the $5d_\delta$ atomic orbitals, and the relatively high excitation energy of the $^{14}\Delta_g$ state reflects strong coupling between the sole unpaired outer-valence electron with the $4f^7$ centers on the Gd atoms. The AFM coupled $^2\Delta$ state (T_0 = 0.14 eV) is the lowest-energy bound excited state found for the anion. The structure of this AFM coupled state and the neutral AFM coupled states (*vide infra*) are calculated to have broken symmetry ($C_{\infty v}$ rather than $D_{\infty h}$ symmetry). Both Gd−O bond lengths are included in Table 2. This geometric symmetry breaking is likely an artifact of the single-determinant structure of our DFT calculations and is due to asymmetric spin polarization. Indeed, with a multideterminantal wave function one would expect equal Gd−O bond distances.

The two bound excited states predicted for Gd_2O^- could increase congestion in the spectrum of Gd_2O^-. However, the additional irregularly spaced partially resolved features in the various bands, and the change in relative intensities of the numerous transitions with photon energy, again point to PEVE interactions that may result in the appearance of two-electron transitions or transitions involving a change in the magnetic coupling between the two Gd $4f^7$ centers.

Neutral Excited States. Nominally one-electron detachment from the σ_u orbital would result in increased but weak bonding between the Gd centers, and calculations on states resulting

https://doi.org/10.1021/acs.jpca.1c07818
J. Phys. Chem. A 2021, 125, 9892−9903

from σ_u detachment are predicted to be bent. Neutral structures that converged in a bent geometry are distinguished by their C_{2v} term symbols in Table 1 (the optimized energy, as well as the energy of the state confined to a linear structure, are included in Table 1). The lowest-energy bent neutral ($\angle$Gd−O−Gd = 106°), a $^{17}B_2$ state, is predicted to lie 0.95 eV above the ground-state anion, and we tentatively assign this transition to **X**.

A transition from the linear anion to this bent neutral state would exhibit an extended progression in the bend mode, which has a calculated harmonic frequency of 100 cm^{-1} and would therefore be unresolved in the experimental spectrum. Figure 4 shows a simulation based on the ADE and VDE

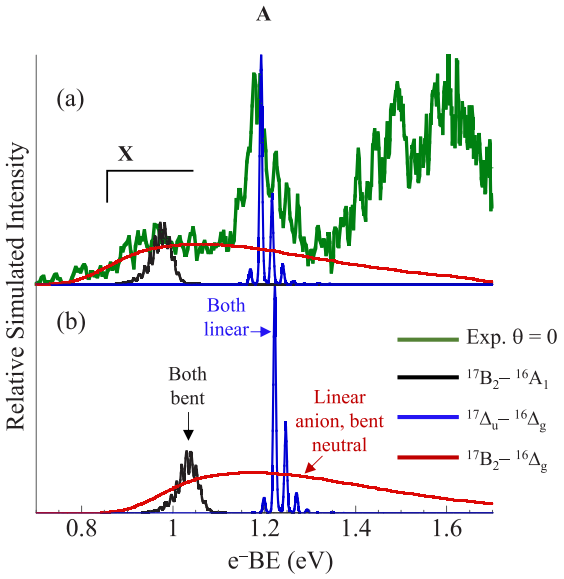

Figure 4. (a) Simulations based on calculated anion and neutral structures. The black trace is based on bent structures for both the anion and neutral; the blue trace is based on the linear structures for both the anion and neutral; the red trace is based on the linear anion and bent neutral. Transition origins have been adjusted to compare with the experimental spectrum (green). (b) Same simulations shown at the calculated transition energies (Table 2).

values calculated for the $^{17}B_2 \leftarrow {}^{16}\Delta_g$ transition (red trace) both with the origin shifted to agree with band **X** transition in the experimental spectrum (green) and at the computed origin (panels a and b, respectively). The progression would necessarily be anharmonic and perturbed by strong vibronic coupling, given the increase in spin−orbit coupling with the more linear structure sampled at higher bend quanta.[54] The VDE value for the $^{17}B_2 \leftarrow {}^{16}\Delta_g$ transition is computationally identical to the energy for the analogous neutral linear state (imaginary bend frequency), which is 1.22 eV. The blue trace shows the simulation based on the hypothetical $^{17}\Delta_u \leftarrow {}^{16}\Delta_g$ transition, which appears similar to band **A**. As a final comparison, a simulation based on the bent structures for both the anion and neutral (black trace) is included; it does not agree with any features in the experimental spectrum, providing further support for the linear anion.

The striking differences in the PE spectra of Gd_2O^- and Ce_2O^- or Sm_2O^- can be attributed to the linear structure of Gd_2O^- and bent structures of Ce_2O^- and Sm_2O^-. Among the three triatomics, only Gd_2O^- has (single) occupancy of every 4f-based molecular orbital, including the least stable $\sigma_{g,4f}$ and $\sigma_{u,4f}$ orbitals in the ligand field of the O atom. Analogous $a_{1,4f}$ and $b_{2,4f}$ orbitals are unoccupied in Ce_2O^- and Sm_2O^-. Gd_2O^- is therefore unique in that configuration interaction between these orbitals, and their like-symmetry $\sigma_{g,6s}$ and $\sigma_{u,6s}$ orbitals may underpin large exchange interactions. A similar rationale has been invoked in studies on a series of organolanthanide complex anion PE spectra.[55−57]

Continuum signal lies between bands **X** and **A**, raising the question of whether strong vibronic coupling between bent and linear neutral states is in evidence. Again, considering the large spin−orbit splitting expected for any linear structure, the linear $^{17}\Delta_u$ could conceivably be a metastable structure with which the linear anion would be structurally similar (*i.e.*, a near-vertical transition). We therefore tentatively assign band **A**, which is nearly vertical, to the $^{17}\Delta_u \leftarrow {}^{16}\Delta_g$ transition. The calculated transition energy (1.22 eV) agrees with the most intense partially resolved feature in this band.

The associated lower-spin $^{15}B_2$ state accessed by detaching the σ_u^α electron (also bent; $\angle$Gd−O−Gd = 105°) is predicted to lie at e⁻BE = 1.30 eV, with a 1.66 eV calculated VDE. The coupling between a single electron in the σ_u orbital with the core-like $4f^7$ electrons is significant, given the predicted 0.35 eV $^{17}B_2$–$^{15}B_2$ splitting. Again, an electron occupies the 5d outer-valence orbital as well, which also couples to the unpaired electron in the b_2 (σ_u) orbital. Unlike the linear $^{17}\Delta_u$ state, which has an imaginary bend frequency, the lower-spin linear $^{15}\Delta_u$ state is a local minimum computed to be 0.36 eV higher in energy than the $^{15}B_2$ structure with the same nominal electronic configuration. The $^{15}B_2 \leftarrow {}^{16}\Delta_g$ transition would again be broadened by an extended vibrational progression in the bend mode, while the $^{15}\Delta_u \leftarrow {}^{16}\Delta_g$ would be nearly vertical. The calculated transition energy of the latter (1.66 eV) is in reasonable agreement with band **C**, which we therefore tentatively assign to the $^{15}\Delta_u \leftarrow {}^{16}\Delta_g$ transition.

The calculated $^{17}\Delta_g$ neutral state, accessed by detaching the σ_g^β electron, increases antibonding between the two Gd centers and therefore results in a stable linear structure; it is predicted to be 1.62 eV above the anion ground state, with the lower spin $^{15}\Delta_g$ (from PIMOM) analogue at 2.04 eV. Taking into account that the calculated $^{17}\Delta_g \leftarrow {}^{16}\Delta_g$ is lower than the calculated $^{15}\Delta_u \leftarrow {}^{16}\Delta_g$, we tentatively assign band **B** to $^{17}\Delta_g \leftarrow {}^{16}\Delta_g$ and band **D** to $^{15}\Delta_u \leftarrow {}^{16}\Delta_g$. These assignments agree well with the calculated $^{15}\Delta$–$^{17}\Delta$ splittings for both the $^{2s+1}\Delta_g$ and $^{2s+1}\Delta_u$ states. However, bands **B**, **C**, and **D** have multiple partially resolved features, some of which have opposite PADs, and the continuum signal and congestion are more prevalent in the experimental PE spectrum collected with lower photon energy.

Two-Electron Transitions. We first consider electronic states that might be accessible *via* shake up (two-electron) transitions that might be prevalent because of PEVE interactions. We conducted a thorough search of electronic states associated with permuting the valence electrons in the states that are one-electron accessible from the $^{16}\Delta_g$ ($\sigma_g^2\sigma_u^2$, $\sigma_g^2\sigma_u\delta_g$, and $\sigma_g\sigma_u^2\delta_g$) to the unoccupied 5d- (δ, π, σ) and 6p- (π, σ) based MOs, which should be low-energy based on the electronic structure of GdO.[58] States that converged in a 3.5 eV energy window are included in Table 2, and additional higher-energy states that converged are included in the Supporting Information. There are numerous states that would be accessed *via* detachment from the σ_u or σ_g orbital coupled with $\delta_u \leftarrow \delta_g$ or $\pi_{6p} \leftarrow \delta_g$ promotion in the 1.5−2.0 eV range. As suggested in a previous study, these transitions would arise from the polarization of outer-valence orbitals by the

https://doi.org/10.1021/acs.jpca.1c07818
J. Phys. Chem. A 2021, 125, 9892−9903

electric field from the departing electron,[13] the outer-valence orbitals being very polarizable.[59] Rigorous theoretical treatment of shakeup transitions can be found in the literature,[60,61] but as a simple heuristic example, an electron ejected along the Gd-O-Gd axis would polarize the electron in the δ_g away from the photoelectron in a way that could be described as $c_1(t)\delta_g + c_2(t)\delta_u$. The final neutral state would therefore have nonzero probability of having a singly occupied δ_u orbital, though the initial state had a singly occupied δ_g orbital. Wang and coworkers observed evidence of a time-independent valence orbital polarization in their anion PE spectra of dipole-bound anionic states.[19]

Several of the states calculated to be in the 1.5−2.0 eV e^-BE range are accessible *via* a one-electron transition from a bound excited state of the anion, which may account for some of the congestion observed in the spectrum. However, the spectra collected with 2.330 and 3.495 eV photon energies were collected under identical ion source conditions. The fact that bands **B**, **C**, and **D** are more intense when compared to band **A** in the spectrum collected with 2.330 eV photon energy than in the 3.495 eV spectrum shows that the spectral congestion increases with decreasing e^-KE, which results in longer PEVE interaction times. Longer interaction times result in an increased population of final states that are accessed by two-electron transitions.[12]

Excited states involving detachment from the σ_g or σ_u orbitals along with promotion of an electron from either the σ_g or σ_u orbital to the δ_g or δ_u orbital are calculated to lie above 2.8 eV. The manifold of transitions labeled **E** may include some of these transitions, but considering the large number of close-lying states predicted to be in this energy range, any specific assignments would be speculative. Anion PE spectra of other lanthanide suboxides exhibit low-intensity features with similar profiles, but at different energies (*e.g.*, band A′ in the PE spectrum of Ce_2O^- shown in Figure 2a).[15,16,42,43,62]

Anomalous Photoelectron Angular Distributions. None of the preceding discussion addresses the curious differences in PAD of features within a given manifold. All anion PE spectra of lanthanide suboxides measured with the experimental apparatus described here have shown the hallmarks of detachment transitions from diffuse molecular orbitals with Ln 6s character, which are large detachment cross sections and parallel PADs. The PE spectrum of Gd_2O^- obtained using 3.495 eV photon energy (Figure 2c), at first glance, appears to have the same characteristics, but closer inspection of this spectrum, in addition to the better-resolved spectrum obtained with 2.330 eV photon energy (Figure 3) shows that several partially resolved features have opposite PADs. Table 1 includes an indication of which partially resolved peaks are more intense in spectra obtained with $\theta = 0$ (∥) and $\theta = \frac{\pi}{2}$ (⊥) laser polarization.

Spin−orbit coupling has been implicated in disparate asymmetry parameters for different final components within a spin−orbit multiplet. Early studies on Cd ($4d^{10}\ 5s^2\ ^1S_0$) atomic ionization processes[63] showed nearly isotropic PAD for transitions to the excited $4d^9\ 5s^2\ ^2D_{3/2}$ state ($\beta = -0.12$), with more a parallel PAD ($\beta = 1.49$) for transitions to the $4d^9\ 5s^2\ ^2D_{5/2}$ state. Subsequent studies by others suggested the possibility that this effect was due to an autoionizing transition and that the actual asymmetries plotted against e^-KE, versus photon energy, were similar.[64,65] Different final states associated with 2p ionization of O atoms showed disparate asymmetry parameters for the ^1D and ^3S cationic states, 0.34 and 0.71, respectively.[66] But, again, these values change dramatically with e^-KE, and the different final states are associated with different e^-KE values for any given photon energy.

In contrast, there are transitions with distinct perpendicular polarization dispersed throughout the spectrum of Gd_2O^-. Parallel transitions, such as those observed in most of the PE spectrum, are consistent with detachment from orbitals with strong 6s character. Given a linear Gd_2O^- anion, detachment from the σ_u or σ_g orbitals will result in no change in orbital angular momentum between the anion and neutral electronic states, giving a selection rule of ΔS, $\Delta M_s = \pm 1/2$. The two sets of $^{17}\Delta \leftarrow {}^{16}\Delta$ ($\Delta M_s = +1/2$) and $^{15}\Delta \leftarrow {}^{16}\Delta$ ($\Delta M_s = -1/2$) transitions fall into this category, and the resulting photoelectron would carry away $l = 1$ unit of angular momentum, consistent with the parallel PAD.[31] From the standpoint of orbital angular momentum, there is no explanation for the features with perpendicular PAD, unless the orbital angular momentum of the ejected electron is affected by PEVE interactions in a way that was not observed in previous studies on similar strongly correlated systems.[13]

Considering the strong coupling between unpaired outer-valence electrons and the $4f^7$ cores evident from the energy associated with $\alpha \rightarrow \beta$ spin flips in the δ orbitals (*ca.* 0.8 eV, Table 1), it is conceivable that there is similarly strong coupling between the orbital angular momentum of the ejected electron and the projection of the spin angular momentum of the $4f^7$cores. Figure 5 shows a schematic of the energies of the individual M_s levels of the $^{16}\Delta_g$ anion ground state, assuming an axial zero field splitting of -20 cm^{-1}, following $E_{M_s} = \left(M_s^2 - \frac{1}{4}\right)D$ for half integer spins, as well as the levels of the $^{17}\Delta_u$ and $^{15}\Delta_u$ states that follow $E_{M_s} = (M_s^2)D$ for integer spins. We assume $D = -20$ cm^{-1}, for the sake of illustration.

From the lowest-energy degenerate levels of the anion, $M_s = \pm 15/2$, the detachment of a single electron from the σ_u orbital would access the $M_s = \pm 8$ levels of the $^{17}\Delta_u$ state or the $M_s = \pm 7$ levels of the $^{15}\Delta_u$ state, given the selection rule noted above. These transitions are represented by green arrows in Figure 4, which also show transitions from excited M_s levels of the anion. If, however, interaction between the photoelectron with $l = 1$ strongly interacts with the coupled $4f^7$ Gd cores in a way that changes the orbital angular momentum of the outgoing electron to $l = 0$, 2, the resulting PAD would be perpendicular,[31] coupled with $\Delta M_s = \pm 1/2 + 1$ (red dotted arrows) or $\Delta M_s = \pm 1/2 - 1$ (blue dotted arrows) transitions. We note here that neither spin nor orbital angular momentum are good quantum numbers, though we will still frame the idea in L−S terms.

The schematic shown in Figure 5 is oversimplified in that it assumes equal axial zero-field splitting for the anion and two neutral states, $D = -20$ cm^{-1}, but this scheme would result in differences in energy between the parallel and perpendicular transitions. The simulation shown in Figure 6a assumes $D = -20$ cm^{-1} for the anion and two neutral states, equal oscillator strength for all transitions, and thermal population of the four lowest excited M_s levels of the anion (*i.e.*, electronic sequence bands, represented in part by the groupings of green, red, and blue arrows in Figure 5). Note that the transitions associated with $\Delta M_s = \pm 1/2 + 1$ (red dotted arrows) can occur only from the excited M_s levels of the anion. The simulation shows that the sequence bands are close in energy and would not be

https://doi.org/10.1021/acs.jpca.1c07818
J. Phys. Chem. A 2021, 125, 9892−9903

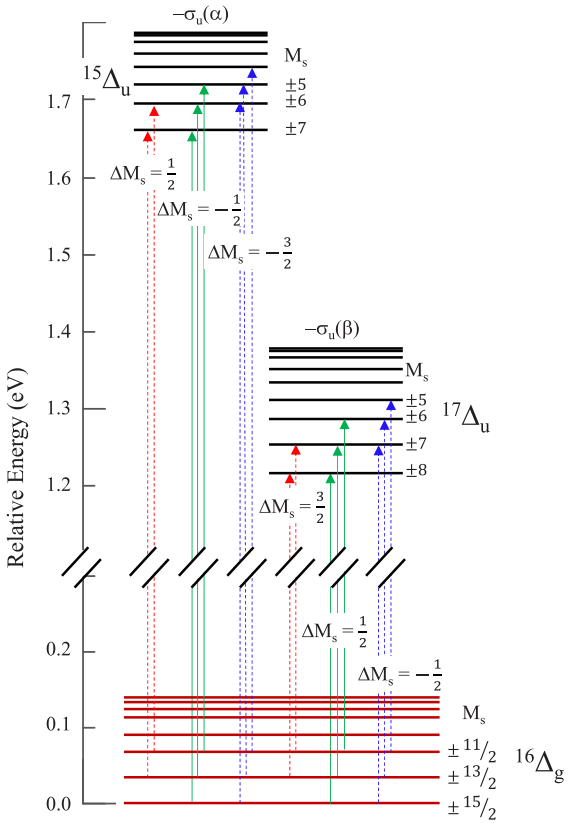

Figure 5. Energies of the M_s levels of the $^{16}\Delta_g$ state of Gd_2O^- and the neutral $^{17}\Delta_u$ and $^{15}\Delta_u$ states accessed by detachment of an electron from the σ_u outer valence orbital. The green arrows show transitions that follow the $\Delta S = +1/2$ (accessing $^{17}\Delta_g$) and $-1/2$ (accessing $^{15}\Delta_g$) selection rule. The blue and red dashed arrows are hypothetically allowed transitions if angular momentum from the $l = 1$ photoelectron generated from detachment from an orbital with zero orbital angular momentum were transferred to change M_s by an additional unit.

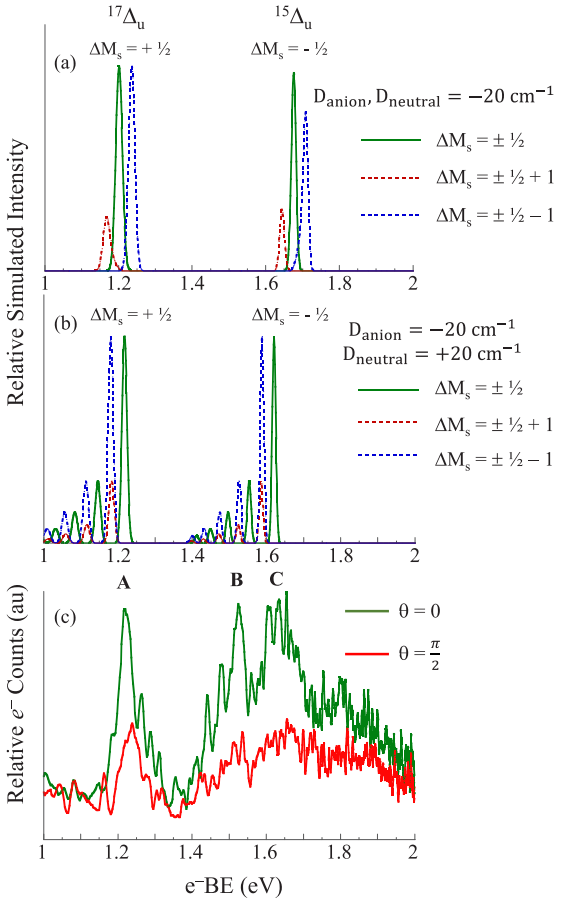

Figure 6. (a) Simulation based on the energy levels shown in Figure 4, assuming thermal population of the 5 lowest-energy M_s levels of the $^{16}\Delta_g$ anion. Color coding of transitions is consistent with the arrows representing the transitions in Figure 4. D is assumed to be $-20\ cm^{-1}$ for the $^{16}\Delta_g$, $^{17}\Delta_g$, and $^{15}\Delta_g$ states. (b) Simulation of the same transitions assuming D is $-20\ cm^{-1}$ for the $^{16}\Delta_g$ state, and $+20\ cm^{-1}$ for the $^{17}\Delta_g$ and $^{15}\Delta_g$ states. ADEs for the transitions based on computed energies for the (unsplit) states. (c) Experimental PE spectrum of Gd_2O^- in the same energy range, for direct comparison to the simulated profiles.

resolved experimentally, but the $l = 0$, 2 perpendicular transitions would appear at lower ($\Delta M_s = \pm1/2 + 1$, dotted red line) and higher ($\Delta M_s = \pm1/2 - 1$, dotted blue line) energies relative to the $l = 1$ ($\Delta M_s = \pm1/2$, green line) parallel transition. The energy interval between the three groups of transitions is dependent on the value of D for the neutral states. Again, note that equal oscillator strength was assumed for all transitions, rather than arbitrarily giving the perpendicular transitions lower oscillator strength. Given these assumptions, the simulation of the $^{17}\Delta_u \leftarrow {}^{16}\Delta_g$ transition resembles band **A** in Figure 6c.

If instead we assume $D = -20\ cm^{-1}$ for the anion and $D = +20\ cm^{-1}$ for the neutral states and apply the same set of selection rules, the simulated transitions appear very different, as shown in Figure 6b. The electronic sequence bands are well separated, trailing to lower e^-BE, and the perpendicular transitions coincide in energy, appearing at lower e^-BE than the parallel transition. The result is similar in appearance to band **B**.

This rationale raises the question of why this phenomenon has not been observed in the spectra of Sm_2O^- or $Gd_2O_2^-$. In both cases, the crowding of electronic transitions made it difficult or impossible to discern features between spectra taken with the different laser polarizations. However, our previously reported PE spectrum of the $MnMoO_3^-$ molecule[49] ($^7A'$ anion ground state) exhibited an anomalous PAD. Figure 7 shows the spectrum near the origin transition obtained using parallel (green) and perpendicular (red) laser polarizations. This relatively narrow electronic transition includes a short vibrational progression, and both the $v' = 0$ and $v' = 1$ members exhibit minima in the perpendicular spectrum where the peaks reach maximum intensity in the parallel spectrum. The S/N in the more intense $v' = 0$ transition is sufficient to determine a splitting of 0.017 eV ($137\ cm^{-1}$) between the partially resolved features in the perpendicular spectrum, which would be consistent with $D = -17\ cm^{-1}$ for neutral $MnMoO_3$.

A more sophisticated theoretical treatment to calculate D for the numerous close-lying electronic states of Gd_2O^- and Gd_2O is beyond the scope of this report. However, the simulations based on values of D in line with those reported for digadolinium complexes in which the Gd centers are bridged by N_2^{3-} ligands[25,26] show profiles that are qualitatively similar to what is observed in the PE spectrum of Gd_2O^-, suggesting that anion PE spectra of these strongly correlated systems could provide another means for modeling potential single-molecule magnet properties.

https://doi.org/10.1021/acs.jpca.1c07818
J. Phys. Chem. A 2021, 125, 9892−9903

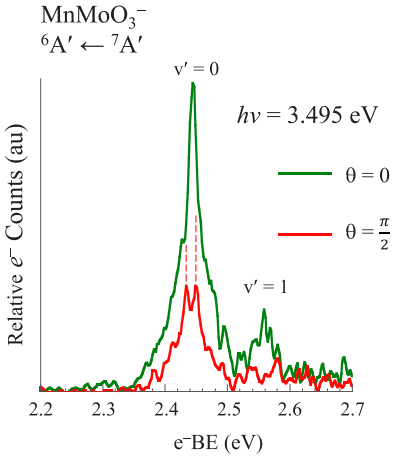

Figure 7. Anion PE spectrum previously reported for $MnMoO_3^-$ measured using 3.495 eV photon energy shown on an expanded scale and with contrasting colors to distinguish between the parallel (green) and perpendicular (red) polarizations. The spectrum obtained with perpendicular polarization shows dips at energies where the parallel spectrum peaks. Reprinted with permission from ref 49. Copyright 2020 AIP Publishing.

CONCLUSIONS

In an extension of our studies on the manifestation of PEVE interactions on the PE spectra of strongly correlated molecular systems, the anion PE spectrum of Gd_2O^- was presented and compared with the Ce_2O^- and Sm_2O^- analogues. The motivation for targeting Gd_2O^- was the expectation of simple electronic structure of the $4f^7$ (^8S) subshell occupancy in Gd atoms, which should reduce the number of close-lying states compared to the numerous spin−orbit components arising from the $4f^6$ (^7F_j) subshell of Sm. On the basis of the analysis of the spectrum with supporting calculations, we conclude the following:

(1) The Gd_2O^- PE spectrum exhibits numerous electronic transitions over a wider range of e⁻BEs compared to the Ce_2O^- and Sm_2O^- spectra. However, like Sm_2O^- the intensities of transitions to excited states increase relative to the ground state with lower photon energy, which is consistent with the hypothesis that the ejected electron creates a time-dependent perturbation of the electronic structure of the neutral Gd_2O remnant, resulting in observation of two-electron (shakeup) transitions.

(2) Calculations predict the linear and bent structures of Gd_2O^- to be nearly identical in energy. However, because of the stability from spin−orbit splitting in the linear $^{16}\Delta_g$ state, we assert that the true ground state is linear.

(3) The group of intense spectral features that lie between 0.7 and 2.3 eV are assigned to transitions involving detachment of an electron from outer-valence σ_u and σ_g orbitals that have large Gd 6s contributions. A very low-intensity transition observed at e⁻BE = 0.26 eV in the spectrum measured with 3.495 eV is assigned to the transition to the ground state *via* detachment of the δ_g (Gd 5d-based) outer-valence electron.

(4) The spectra show parallel transition manifolds in general, which is consistent with detachment from σ_u and σ_g orbitals. However, several distinct perpendicular transitions are observed adjacent to several of the vertical transitions. A possible explanation invoking interaction between the ejected electron and the high-spin neutral is proposed. Specifically, the angular momentum of electrons ejected from σ_u or σ_g orbitals, which is $l = 1$, can be switched to $l = 0$, 2 with an associated change in the M_s of the remnant neutral, which would be spin−orbit coupling between a free electron and the spin of a neutral.

Evidence of strong time-dependent electron−neutral coupling continues to challenge how we envision photodetachment and provides interesting directions for theory.

ASSOCIATED CONTENT

Supporting Information

The Supporting Information is available free of charge at https://pubs.acs.org/doi/10.1021/acs.jpca.1c07818.

DFT-predicted relative energies of 17-tet, 15-tet, 13-tet states of neutral Gd_2O; DFT-predicted relative energies of 16-tet and 14-tet states of Gd_2O^-, including states embedded in the detachment continuum (PDF)

AUTHOR INFORMATION

Corresponding Authors

Hrant P. Hratchian − *Department of Chemistry and Biochemistry, University of California, Merced, Merced, California 95343, United States;* orcid.org/0000-0003-1436-5257; Email: hhratchian@ucmerced.edu

Caroline Chick Jarrold − *Department of Chemistry, Indiana University, Bloomington, Indiana 47405, United States;* orcid.org/0000-0001-9725-4581; Email: cjarrold@indiana.edu

Authors

Jarrett L. Mason − *Department of Chemistry, Indiana University, Bloomington, Indiana 47405, United States*

Hassan Harb − *Department of Chemistry and Biochemistry, University of California, Merced, Merced, California 95343, United States*

Ali Abou Taka − *Department of Chemistry and Biochemistry, University of California, Merced, Merced, California 95343, United States;* orcid.org/0000-0003-0001-2813

Caleb D. Huizenga − *Department of Chemistry, Indiana University, Bloomington, Indiana 47405, United States*

Hector H. Corzo − *Department of Chemistry and Biochemistry, University of California, Merced, Merced, California 95343, United States*

Complete contact information is available at: https://pubs.acs.org/10.1021/acs.jpca.1c07818

Notes

The authors declare no competing financial interest.

The data supporting the findings of this study are available from the corresponding authors upon request.

ACKNOWLEDGMENTS

C.C.J. and H.P.H. are grateful for insightful comments from the reviewers. C.C.J. is grateful for support from the Indiana University College of Arts and Sciences. H.P.H. is grateful for generous support from the National Science Foundation (CHE-1848580) and acknowledges computing time on the Multi-Environment Computer for Exploration and Discovery (MERCED) cluster which was supported by the National Science Foundation (Grant No. ACI-1429783).

REFERENCES

(1) Aromí, G.; Agulià, D.; Gamez, P.; Luis, F.; Roubeau, O. Design of Magnetic Coordination Complexes for Quamtum Computing. *Chem. Soc. Rev.* **2012**, *41*, 537−546.

(2) Clemente-Juan, J. M.; Coronado, E.; Gaita-Ariña, A. Magnetic Polyoxometalates: From Molecular Magnetism to Molecular Spintronics and Quantum Computing. *Chem. Soc. Rev.* **2012**, *41*, 7464−7478.

(3) Aguilà, D.; Barrios, L. A.; Velasco, V.; Roubeau, O.; Repollés, A.; Alonso, P. J.; Sese, J.; Teat, S. J.; Luis, F.; Aromí, G. Heterodimetallic [LnLn′] Lanthanide Complexes: Toward a Chemical Desicng of Two-Qubit Molecular Spin Quantum Gates. *J. Am. Chem. Soc.* **2014**, *136*, 14215−14222.

(4) Trabesinger, A. Quantum Leaps, Bit by Bit. *Nature* **2017**, *543*, S2−S3.

(5) Barnes, S. E.; Ieda, J.; Maekawa, S. Rashba Spin-Orbit Anisotropy and the Electric Field Control of Magnetism. *Sci. Rep.* **2015**, *4*, 4105.

(6) Zhou, Z.; Trassin, M.; Gao, Y.; Gao, Y.; Qiu, D.; Ashraf, K.; Nan, T.; Yang, X.; Bowden, S. R.; Pierce, T. D. Probing Electric Field Control of Magnetism using Ferromagnetic Resonances. *Nat. Commun.* **2015**, *6*, 6082.

(7) Gould, C. A.; McClain, K. R.; Yu, J. M.; Groshens, T. J.; Furche, F.; Harvey, B. G.; Long, J. R. Synthesis and Magnetism of Neutral, Linear Metallocene Complexes of Terbium(II) and Dysprosium(II). *J. Am. Chem. Soc.* **2019**, *141*, 12967−12973.

(8) Tokmachev, A. M.; Averyanov, D. V.; Taldenkov, A. N.; Parfenov, O. E.; Karateev, I. A.; Sokolov, I. S.; Storchak, V. G. Lanthanide f^7 metalloxenes- A Class of Intrinsic 2D Ferromagnets. *Mater. Horiz.* **2019**, *6*, 1488−1496.

(9) Field, R. W. Diatomic Molecule Electronic Structure beyond Simple Molecular Constants. *Ber. Bunsenges. Phys. Chem.* **1982**, *86*, 771−779.

(10) Kaledin, L. A.; McCord, J. E.; Heaven, M. C. Laser Spectroscopy of CeO- Characterization and Assignment of States in the 0−3 eV Range. *J. Mol. Spectrosc.* **1993**, *158*, 40−61.

(11) Kaledin, L. A.; McCord, J. E.; Heaven, M. C. Rotation-Electronic Depurturbation Analysis of the 4f 6s Configurational States of CeO. *J. Mol. Spectrosc.* **1995**, *170*, 166−171.

(12) Mason, J. L.; Topolski, J. E.; Ewigleben, J. C.; Iyengar, S. S.; Jarrold, C. C. Photoelectrons Are Not Always Quite Free. *J. Phys. Chem. Lett.* **2019**, *10*, 144−149.

(13) Mason, J. L.; Harb, H.; Taka, A. A.; McMahon, A. J.; Huizenga, C. D.; Corzo, H.; Hratchian, H. P.; Jarrold, C. C. Photoelectron Spectra of $Gd_2O_2^-$ and Nonmonotonic Photon- Energy-Dependent Variations in Populations of Close-Lying Neutral States. *J. Phys. Chem. A* **2021**, *125*, 857−866.

(14) Wigner, E. P. On the Behavior of Cross Sections Near Thresholds. *Phys. Rev.* **1948**, *73*, 1002−1009.

(15) Kafader, J. O.; Topolski, J. E.; Marrero-Colon, V.; Iyengar, S. S.; Jarrold, C. C. The Electron Shuffle: Cerium Influences Samarium 4f Orbital Occupancy in Heteronuclear Ce-Sm Oxide Clusters. *J. Chem. Phys.* **2017**, *146*, 194310.

(16) Topolski, J.E.; Kafader, J.O.; Marrero Colon, V.; Iyengar, S.S.; Hratchian, H.P.; Jarrold, C.C. Exotic Electronic Structures of $Sm_xCe_{3-x}O_y$ (x = 0−3; y = 2−4) Clusters and the Effect of High Neutral Density of Low-Lying States on Photodetachment Transition Intensities. *J. Chem. Phys.* **2018**, *149*, 054305.

(17) Weichman, M. L.; Vlaisavljevich, B.; DeVine, J. A.; Shuman, N. S.; Ard, S. G.; Shiozaki, T.; Neumark, D. M.; Viggiano, A. A. Electronic Structure of SmO and SmO^- via Slow Photoelectron Velocity-Map Imaging Spectroscopy and Spin-Orbit CASPT2 Calculations. *J. Chem. Phys.* **2017**, *147*, 234311.

(18) Furet, E.; Costuas, K.; Rabiller, P.; Maury, O. On the Sensitivity of f Electrons to Their Chemical Environment. *J. Am. Chem. Soc.* **2008**, *130*, 2180−2183.

(19) Yuan, D.-F.; Liu, Y.; Qian, C.-H.; Kocheril, G. S.; Zhang, Y.-R.; Rubenstein, B. M.; Wang, L.-S. Polarization of Valence Orbitals by the Intramolecular Electric Field from a Diffuse Dipole-Bound Electron. *J. Phys. Chem. Lett.* **2020**, *11*, 7914−7919.

(20) Fechner, M.; Zahn, P.; Ostanin, S.; Bibes, M.; Mertig, I. Switching Magnetization by 180° with an Electric Field. *Phys. Rev. Lett.* **2012**, *108*, 197206.

(21) Yun, K.-H.; Lee, M.; Chung, Y.-C. Electric Field as a Novel Switch for Magnetization of Fe/Graphene System. *J. Magn. Magn. Mater.* **2014**, *362*, 93−96.

(22) Wang, W.-G.; Li, M.; Hageman, S.; Chien, C. L. Electric-Field-Assisted Switching in Magnetic Tunnel Junctions. *Nat. Mater.* **2012**, *11*, 64−68.

(23) Negulyaev, N. N.; Stepanyuk, V. S.; Hergert, W.; Kirschner, J. Electric Field as a Switching Tool for Magnetic States in Atomic-Scale Nanostructures. *Phys. Rev. Lett.* **2011**, *106*, 037202.

(24) Costes, J. P.; Dahan, F.; Nicodeme, F. A Trinuclear Gadolinium Complex: Structure and Magnetic Properties. *Inorg. Chem.* **2001**, *40*, 5285−5287.

(25) Rinehart, J. D.; Fang, M.; Evans, W. J.; Long, J. R. Strong Exchange and Magnetic Blocking in N_2^{3-} Radical-Bridged Lanthanide Complexes. *Nat. Chem.* **2011**, *3*, 538−542.

(26) Meihaus, K. R.; Corbey, J. F.; Fang, M.; Ziller, J. W.; Long, J. R.; Evans, W. J. Influence of an Inner-Sphere K+ Ion on the Magnetic Behavior of N_2^{3-} Radical-Bridged Dilanthanide Complexes Isolated Using an External Magnetic Field. *Inorg. Chem.* **2014**, *53*, 3099−3107.

(27) Moravec, V. D.; Jarrold, C. C. Study of the Low-Lying States of NiO^- and NiO using Anion Photoelectron Spectroscopy. *J. Chem. Phys.* **1998**, *108*, 1804−1810.

(28) Waller, S. E.; Mann, J. E.; Jarrold, C. C. Asymmetric Partitioning of Metals among Cluster Anions and Cations Generated via Laser Ablation of Mixed Aluminum/Group 6 Transition Metal Targets. *J. Phys. Chem. A* **2013**, *117*, 1765−1772.

(29) Felton, J. A.; Ray, M.; Jarrold, C. C. Measurement of the Electron Affinity of Atomic Ce. *Phys. Rev. A: At., Mol., Opt. Phys.* **2014**, *89*, 033407.

(30) Baker, J. M. B. Beam Modulated Time-of-Flight Mass Spectrometry. II. Experimental Work. *J. Phys. E: Sci. Instrum.* **1974**, *7*, 364−368.

(31) Sanov, A. Laboratory-Frame Photoelectron Angular Distributions in Anion Photodetachment: Insight into Electronic Structure and Intermolecular Interactions. *Annu. Rev. Phys. Chem.* **2014**, *65*, 341−363.

(32) Frisch, M. J.; Trucks, G. W.; Schlegel, H. B.; Scuseria, G. E.; Robb, M. A.; Cheeseman, J. R.; Scalmani, G.; Barone, V.; Petersson, G. A.; Nakatsuji, H.; et al. *Gaussian 16*; Gaussian Inc.: Wallingford, CT, United States, 2016.

(33) Cao, X.; Dolg, M. Valence Basis Sets for Relativistic Energy-Consistent Small-Core Lanthanide Pseudopotentials. *J. Chem. Phys.* **2001**, *115*, 7348−7355.

(34) Dunning, T. H. Gaussian-Basis Sets for use in Correlated Molecular Calculations. 1. The Atoms Boron through Neon and Hydrogen. *J. Chem. Phys.* **1989**, *90*, 1007−1023.

(35) Seeger, R.; Pople, J. A. Self-Consistent Molecular Orbital Methods. 18. Constraints and Stability in Hartree-Fock Theory. *J. Chem. Phys.* **1977**, *66*, 3045−3050.

(36) Bauernschmitt, R.; Ahlrichs, R. Stability Analysis for Solutions of the Closed Shell Kohn-Sham Equation. *J. Chem. Phys.* **1996**, *104*, 9047−9052.

(37) Gilbert, A. T. B.; Besley, N. A.; Gill, P. M. W. Self-Consistent Field Calculations of Excited States Using the Maximum Overlap Method (MOM). *J. Phys. Chem. A* **2008**, *112*, 13164−13171.

(38) Barca, G. M.; Gilbert, A. T. B.; Gill, P. M. W. Simple Models for Difficult Electronic Excitations. *J. Chem. Theory Comput.* **2018**, *14*, 1501−1509.

(39) Frisch, M. J.; Trucks, G. W.; Schlegel, H. B.; Scuseria, G. E.; Robb, M. A.; Cheeseman, J. R.; Scalmani, G.; Barone, V.; Petersson, G. A.; Nakatsuji, H.; et al. *Gaussian Development Version, Revision J.15*; Gaussian, Inc.: Wallingford, CT, 2020.

(40) Schaugaard, R. N.; Topolski, J. E.; Ray, M.; Raghavachari, K.; Jarrold, C. C. Insight into Ethylene Interactions with Molybdenum

https://doi.org/10.1021/acs.jpca.1c07818
J. Phys. Chem. A 2021, 125, 9892−9903

Suboxide Cluster Anions from Photoelectron Spectra of Chemifragments. *J. Chem. Phys.* **2018**, *148*, 054308.
(41) Cotton, S. *Lanthanide and Actinide Chemistry*; John Wiley & Sons, Ltd., 2006.
(42) Kafader, J. O.; Topolski, J. E.; Jarrold, C. C. Molecular and Electronic Structures of Cerium and Cerium Suboxide Clusters. *J. Chem. Phys.* **2016**, *145*, 154306.
(43) Ray, M.; Felton, J. A.; Kafader, J. O.; Topolski, J. E.; Jarrold, C. C. Photoelectron Spectra of CeO^- and $Ce(OH)_2^-$. *J. Chem. Phys.* **2015**, *142*, 064305.
(44) Kafader, J. O.; Ray, M.; Jarrold, C. C. Photoelectron Spectrum of PrO^-. *J. Chem. Phys.* **2015**, *143*, 064305.
(45) Nakajima, T.; Hirao, K. The Douglas-Kroll-Hess Approach. *Chem. Rev.* **2012**, *112*, 385−402.
(46) Becke, A. D. Density-Functional Thermochemistry. IV. A New Dynamical Correlation Functional and Implications for Exact-Exchange Mixing. *J. Chem. Phys.* **1996**, *104*, 1040−1046.
(47) Topolski, J. E.; Kafader, J. O.; Ray, M.; Jarrold, C. C. Elucidating Cerium + H_2O Reactivity through Electronic Structure: A Combined PES and DFT Study. *J. Mol. Spectrosc.* **2017**, *336*, 1−11.
(48) Topolski, J. E.; Kafader, J. O.; Jarrold, C. C. Ce in the + 4 Oxidation State: Anion Photoelectron Spectroscopy and Photodissociation of Small CexOyHz− molecules. *J. Chem. Phys.* **2017**, *147*, 104303.
(49) Mason, J. L.; Gupta, A. K.; McMahon, A. J.; Folluo, C. N.; Raghavachari, K.; Jarrold, C. C. The Striking Influence of Oxophilicity Differences in Heterometallic Mo-Mn Oxide Cluster Reactoins with Water. *J. Chem. Phys.* **2020**, *152*, 054301.
(50) Mann, J. E.; Mayhall, N. J.; Jarrold, C. C. Properties of Metal Oxide Clusters in non-Traditional Oxidation States. *Chem. Phys. Lett.* **2012**, *525*−*526*, 1.
(51) Kramida, A.; Ralchenko, Y.; Reader, J.; NIST ASD Team. *NIST Atomic Spectra Database* (ver 5.8). https://physics.nist.gov/asd (2021, February 11). National Institute of Standards and Technology: Gaithersburg, MD, 2020. DOI: 10.18434/T4W30F.
(52) Beck, D. R.; O'Maley, S. M.; Pan, L. In *Computational Methods in Lanthanide and Actinide Chemistry*; Dolg, M., Ed.; Wiley: Chichester, 2015; p 11.
(53) O'Malley, S. M.; Beck, D. R. Calculation of Ce- Binding Energies by Analysis of Photodetachment Partial Cross Sections. *Phys. Rev. A: At., Mol., Opt. Phys.* **2006**, *74*, 042509.
(54) Mann, J. E.; Waller, S. E.; Rothgeb, D. W.; Jarrold, C. C. Resonant Two-Photon Detachment of WO_2^-. *Chem. Phys. Lett.* **2011**, *506*, 31−36.
(55) Hosoya, N.; Yada, K.; Masuda, T.; Nakajo, E.; Yabushita, S.; Nakajima, A. Investigation of the Electronic Structures of Organolanthanide Sandich Complex Anions by Photoelectron Spectroscopy: 4f Orbital Contribution in the Metal-Ligand Interaction. *J. Phys. Chem. A* **2014**, *118*, 3051−3060.
(56) Nakajo, E.; Masuda, T.; Yabushita, S. Theoretical Study on the Photoelectron Spectra of $Ln(COT)_2^-$: Lanthanide Dependence of the Metal-Ligand Interaction. *J. Phys. Chem. A* **2016**, *120*, 9529−9544.
(57) Nakajo, E.; Yabushita, S. Theoretical Study on the Anion Photoelectron Spectra of $Ln(COT)_2^-$ Including Spin-Orbit Effects. *Chem. Phys. Lett.* **2017**, *678*, 259−264.
(58) Kaledin, L. A.; Erickson, M. G.; Heaven, M. C. Laser Spectroscopy of GdO- Ligand-Field Assignments of $4f^7$ (^8S) 6p − $4f^7$ (^8S) 6s Transitions. *J. Mol. Spectrosc.* **1994**, *165*, 323−333.
(59) Gotkis, I. Field-Stimulated Electron Promotion from Core 4f Orbital to Out-of-Core σ_{6s} Orbital Phenomenon in Simple Lanthanide Compounds. *J. Phys. Chem.* **1991**, *95*, 6086−6095.
(60) Martin, R. L.; Shirley, D. A. Theory of Core-Level Photoemission Correlation State Spectra. *J. Chem. Phys.* **1976**, *64*, 3685−3689.
(61) Arneberg, R.; Muller, J.; Manne, R. Configuration Interaction Calculations of Satellite Structure in Photo-Electron Spectra of H_2O. *Chem. Phys.* **1982**, *64*, 249−258.
(62) Klingeler, E.; Pontius, N.; Lüttgens, G.; Bechthold, P. S.; Neeb, M.; Eberhardt, W. Photoelectron Spectroscopy of GdO^-. *Phys. Rev. A: At., Mol., Opt. Phys.* **2002**, *65*, 032502.
(63) Harrison, H. Angular Distribution of Photoelectron. I. Cadmium and Zinc Atoms at 584 and 1048 Å. *J. Chem. Phys.* **1970**, *52*, 901−905.
(64) Walker, T. E. H.; Waber, J. T. Spin-Orbit Coupling and Photoionization. *J. Phys. B: At. Mol. Phys.* **1974**, *7*, 674−692.
(65) Schonhense, G.; Schafers, F.; Heinzmann, U.; Kessler, J. Angle- and Spin-Resolved Photoelectron Spectroscopy of the Hg $5d^{10}$ Subshell. *Z. Phys. A: At. Nucl.* **1982**, *304*, 31−40.
(66) Samson, J. A. R.; Hancock, W. H. Angular Distribution of Photoelectrons from Atomic Oxygen at 736 Å and 584 Å. *Phys. Lett. A* **1977**, *61A*, 380−382.

https://doi.org/10.1021/acs.jpca.1c07818
J. Phys. Chem. A 2021, 125, 9892−9903